Models for solidification and splashing in laser percussion drilling

Models for solidification and splashing in laser percussion drilling

W. R. Smith
Department of Mathematics and Computing Science, Technische Universiteit Eindhoven, PO Box 513, 5600 MB Eindhoven, The Netherlands

Abstract. This paper studies systems of partial differential equations modelling laser percussion drilling. The particular phenomenon considered in detail is the ejection of the thin layer of molten material. This thin layer is modelled as an inviscid flow between the fluid surface and fluid/solid interface, both of which are unknown moving boundaries. Through a regular asymptotic expansion, the governing equations are reduced to a combination of the shallow water equations and a two-phase Stefan problem; the key small parameter being the square of the aspect ratio. These leading-order problems exhibit shocks which represents a possible mechanism for the previously unexplained fluid clumping. Approximate formulas and a parameter grouping are derived to predict the rate of melt solidification during ejection. Finally, weak formulations of the convection-diffusion equation for energy conservation are presented. These weak formulations are novel because the energy equation in the fluid contains convection terms. An appropriate extension to the enthalpy method is suggested as a first stage towards numerical calculations.

Keywords. laser percussion drilling, mathematical modelling, weak formulations

AMS(MOS) subject classifications. 35R35, 80A22

1 Introduction

Laser percussion drilling is used to machine gas turbine components which are typically made out of superalloys; these materials cannot be machined with conventional mechanical drills. The term percussion refers to the repeated operation of the laser in short pulses (10^{-3}s) which are separated by longer time periods (10^{-2}s). The laser builds up energy at a bounded rate and operation in this manner allows for large bursts of energy. Percussion drilling is favoured over other processes, such as spark erosion drilling or laser trepanning drilling, because it is by far the quickest. However, it suffers from three drawbacks (i) recast; solidified material at the wall of the hole, (ii) tapering; decrease of hole diameter with depth and (iii) bellow shape; local increase of hole diameter. Experimental results have also shown that the penetration depth is limited.

In laser percussion drilling, the metal is ablated by a combination of evaporation and melt ejection. However, the mass fraction extracted by evaporation is typically less than a tenth of the total mass loss [1, p. 133]. The melt ejection can be split into three different stages. Initially a thin region of molten metal is formed by the absorption of laser energy at the target surface. Eventually, the irradiated surface reaches the vaporisation temperature. A splash occurs in which the molten metal is pushed radially by the pressure gradients generated by the sudden expansion of the vapour evaporating from the surface (see the photographs of the early stages of melt ejection [1, p. 133]). The high recoil pressures involved also cause significant variation in the vaporisation temperature and rapid flow of the vapour and air away from the irradiated surface. The molten metal now has a high velocity and it can escape from the hole. However, this liquefied material can resolidify before it escapes from the hole. The walls of the hole are relatively cold and large temperature gradients occur across the thin film. The solid metal left exposed after the splash now starts to absorb laser energy and so on. The time-scales for these three stages are between 10^{-5} s and 10^{-4}s for melting, 10^{-5}s for splashing and solidification. We therefore expect between 10 and 100 splashes within a

10^{-3}s pulse. In this paper, we will be concerned with developing models for solidification of the thin film as it moves along the side wall of the hole and splashing at the base of the hole.

A series of photographs of a hole machined by laser percussion drilling is shown in Figure 1. The number denotes the number of pulses used to create the hole. The growth rate of the hole is initially constant but slows in the later photographs. The eleventh hole appears to be not as deep as the tenth, because the melt pool has solidified at the base of the hole. We note that the seventh and subsequent photographs show the resolidified material on the wall of the hole. This resolidification may be in the form of very thin layers or clumps. In the last three photographs molten metal will have escaped via the bottom exit.

The subject of laser percussion drilling has been studied by several authors (see [6] and references therein). The models take the form of incompressible Navier-Stokes equations including gravity. These equations are currently exclusively solved by numerical approaches, which require extensive computing resources [7]. In this paper, we employ perturbation methods to simplify the models retaining only the most significant physical effects. In particular, we note that the depth of the melt pool is typically of the order of 10^{-4}m ($k(T_v - T_m)/I_t \sim 10^{-4}$m where I_t is the typical laser intensity and the other parameters are given in Table 1) whereas the radius is typically of the order of 10^{-3}m. We will take full advantage of this small aspect ratio.

In the process of melt ejection the Reynolds number is typically much greater than 10^3; the typical values being described below. The fluid flow will be turbulent consisting of eddies of many different scales. It is common practice to use empirical models to describe such flows (see, for example, river flow [4, p. 254]). However, we use a thin-film approximation to inviscid irrotational flow to derive a simplified model similar to the well-established shallow water equations. The leading-order problems also incorporate a two-phase Stefan problem (see [3]). The equations developed in the inviscid limit of laminar flow, which represent conservation of mass, momentum and energy, will be assumed to also describe the averaged behaviour of the turbulent flow. We do not incorporate a friction law due to the experimentally observed high output velocity of the melt from the hole. The high output velocity indicates the melt is not retained in the hole due to momentum loss, but by solidification.

In the absence of experimental data, it is not possible to say whether or not the superalloys under consideration melt and solidify over a range of temperatures. The laser percussion drilling of aluminium will be considered here, aluminium is known to have a single melting point. Therefore, mushy regions will not be considered.

The purpose of this paper is to gain a better understanding of the process of laser percussion drilling. We derive a variety of models for the splash and the melt ejection immediately following the splash. The eventual aim is to select parameters to minimise the three drawbacks associated with laser percussion drilling. The process depends on the material properties, ambient conditions and laser characteristics.

The contents of the paper will now be outlined. The dimensionless parameters are calculated in Section 2. Mathematical models for solidification and splashing are then formulated on the basis of the parameter values. Through a regular asymptotic expansion, the leading-order problems are derived in Section 3; the small parameters being the square of the aspect ratio and the reciprocal of the Stefan number for vaporisation. Shocks occur and appropriate Rankine-Hugoniot relations are deduced. Section 4 describes two approximate analytical solutions to the leading-order problem for solidification: a similarity transformation in the large-time limit (corresponding to deep holes) and a singular asymptotic expansion in the limit of small diffusion. We determine that in the absence of shocks, other than the leading-edge shock, the resolidified material grows parabolically in the large-time limit. In the case of small diffusion, an analytical expression for the growth of the resolidification is obtained. In Section 5, weak formulations for the conservation of energy equations are deduced which are consistent with the Stefan condition at the fluid/solid interface. These weak formulations are unusual because the energy equation in the fluid contains convection terms. An appropriate extension to the enthalpy method is suggested as a first stage towards numerical calculations. Finally, Section 6 gives a

brief discussion of the results.

2 Problem formulation

2.1 Parameter régimes

The different parameters in the model depend on laser set-up, the material to be drilled and the temperature, which for aluminium may vary from 300K to approximately 2500K. For the drilling of aluminium the parameters are given in Table 1 (see, for example, [12]). With a length-scale of $L \sim 10^{-3}$m and thickness $d \sim 10^{-4}$m, a typical aspect ratio is given by $\delta = d/L \sim 0.1$. Of course the aspect ratio changes considerably during the ejection of the melt and the variation in viscosity can result in deviation in the Reynolds number. With a typical maximum velocity given by $U \sim 50\text{ms}^{-1}$ (see [1, p. 132]), the dimensionless parameters are

$$Re = \frac{\rho UL}{\mu} \sim 5 \times 10^4, \quad Fr = \frac{U^2}{Lg} \sim 3 \times 10^5, \quad Pe = \frac{\rho cUL}{k} \sim 5 \times 10^2,$$

$$Br = \frac{\mu U^2}{k(T_v - T_m)} \sim 2 \times 10^{-5}, \quad We = \frac{\rho U^2 L}{\sigma} \sim 7 \times 10^3,$$

where g is the acceleration due to gravity. The order of the parameters motivates us to consider inviscid flow with heat convection and conduction, neglecting viscous boundary layers, surface tension and gravity. Moreover, we assume that the vorticity is initially zero, so that we may consider irrotational flow.

The melt ejection is considered axisymmetric. The radius of curvature of the melt is so much larger than the melt thickness, that we will work in a planar representation for the solidification model and axisymmetric representation for the splashing model. We note that these models only describe the situation when the fluid is present. If the fluid is absent, then the standard heat equation is appropriate.

In the splashing model, we make the simplifying assumption that the entire fluid surface is at vaporisation temperature. However, it may well be the case that only a fraction of the fluid surface is at vaporisation temperature and a mixed boundary value problem must then be studied.

2.2 Solidification model

We consider an incompressible fluid contained in the vertical direction by a bottom defined by $y = \eta(x,t)$ and a top defined by $y = h(x,t)$ as indicated in Figure 2, where x and y are the coordinates in the horizontal (along the side wall) and vertical (perpendicular to the side wall) directions and t is time. Solidified material is present in the region $y < \eta(x,t)$. The initial boundary value problem for the potential $\phi(x,y,t)$, temperature $T(x,y,t)$ and unknown free surfaces $y = \eta(x,t)$ and $y = h(x,t)$ is

$$\nabla^2\phi = 0, \quad \frac{\partial T}{\partial t} + \boldsymbol{\nabla}\phi\cdot\boldsymbol{\nabla}T = \frac{k}{\rho c}\nabla^2 T \quad \text{for} \quad \eta(x,t) < y < h(x,t), \tag{1}$$

$$\frac{\partial T}{\partial t} = \frac{k}{\rho c}\nabla^2 T \quad \text{for} \quad y < \eta(x,t), \tag{2}$$

$$\frac{D}{Dt}(y-h) = 0, \quad \frac{\partial \phi}{\partial t} + \frac{1}{2}|\boldsymbol{\nabla}\phi|^2 = 0, \quad \boldsymbol{\nabla}T\cdot\boldsymbol{\nabla}(y-h) = 0 \quad \text{on} \quad y = h(x,t). \tag{3}$$

$$T = T_m, \quad \boldsymbol{\nabla}\phi\cdot\boldsymbol{\nabla}(y-\eta) = 0, \quad \rho L_f \frac{\partial \eta}{\partial t} + [k\boldsymbol{\nabla}T]_{\eta^-}^{\eta^+}\cdot\boldsymbol{\nabla}(y-\eta) = 0 \quad \text{on} \quad y = \eta(x,t), \tag{4}$$

$$T \to T_a \quad \text{as} \quad y \to -\infty, \tag{5}$$

where T_a is the ambient temperature and the differential operator $\boldsymbol{\nabla} = (\partial/\partial x, \partial/\partial y)$. The first boundary condition in (3) is the conservation of mass, the second conservation of momentum and the third conservation

of energy. The first boundary condition in (4) is the melting isotherm, the second conservation of mass and the third conservation of energy. The conservation of mass and energy boundary conditions have been derived from the general formulations (see [2]).

We transform to dimensionless variables via $\phi = UL\hat{\phi}$, $T = T_m + (T_v - T_m)\hat{T}$, $\eta = d\hat{\eta}$, $h = d\hat{h}$, $x = L\hat{x}$, $y = d\hat{y}$ and $t = L\hat{t}/U$, where T_v is the vaporisation temperature at one atmosphere pressure. The solidification model then becomes (and without ambiguity the hats on the non-dimensional variables can be omitted)

$$\frac{\partial^2\phi}{\partial x^2} + \frac{1}{\delta^2}\frac{\partial^2\phi}{\partial y^2} = 0, \quad \frac{\partial T}{\partial t} + \frac{\partial\phi}{\partial x}\frac{\partial T}{\partial x} + \frac{1}{\delta^2}\frac{\partial\phi}{\partial y}\frac{\partial T}{\partial y} = D\left(\delta^2\frac{\partial^2 T}{\partial x^2} + \frac{\partial^2 T}{\partial y^2}\right) \quad \text{for} \quad \eta(x,t) < y < h(x,t), \tag{6}$$

$$\frac{\partial T}{\partial t} = D\left(\delta^2\frac{\partial^2 T}{\partial x^2} + \frac{\partial^2 T}{\partial y^2}\right) \quad \text{for} \quad y < \eta(x,t), \tag{7}$$

$$\frac{1}{\delta^2}\frac{\partial\phi}{\partial y} = \frac{\partial h}{\partial t} + \frac{\partial\phi}{\partial x}\frac{\partial h}{\partial x}, \quad \frac{\partial\phi}{\partial t} + \frac{1}{2}\left(\left(\frac{\partial\phi}{\partial x}\right)^2 + \frac{1}{\delta^2}\left(\frac{\partial\phi}{\partial y}\right)^2\right) = 0, \quad \frac{\partial T}{\partial y} = \delta^2\frac{\partial h}{\partial x}\frac{\partial T}{\partial x} \quad \text{on} \quad y = h(x,t). \tag{8}$$

$$T = 0, \quad \frac{1}{\delta^2}\frac{\partial\phi}{\partial y} = \frac{\partial\phi}{\partial x}\frac{\partial\eta}{\partial x}, \quad \lambda_f\frac{\partial\eta}{\partial t} + D\left[\frac{\partial T}{\partial y} - \delta^2\frac{\partial\eta}{\partial x}\frac{\partial T}{\partial x}\right]_{\eta^-}^{\eta^+} = 0 \quad \text{on} \quad y = \eta(x,t), \tag{9}$$

$$T \to \bar{T}_a \quad \text{as} \quad y \to -\infty. \tag{10}$$

The dimensionless constants δ, D, λ_f and $\bar{T}_a$ are defined, and typical values given in Table 2; the constraint $\delta^2 \ll 1$ typically holds in practice. The model is regularly perturbed in this small parameter. The parameter λ_f represents the Stefan number for fusion.

2.3 Splashing model

The same notation for potential, temperature and the moving boundaries will be adopted for the splashing model; these quantities are defined anew. We consider an incompressible fluid contained in the vertical direction by a bottom defined by $z = \eta(r,t)$ and a top defined by $z = h(r,t)$ as indicated in Figure 3, where r and z are the coordinates in the radial and vertical directions and t is time. Solidified material is present in the region $z < \eta(r,t)$. The initial boundary value problem for the potential $\phi(r,z,t)$, temperature $T(r,z,t)$ and unknown free surfaces $z = \eta(r,t)$ and $z = h(r,t)$ is

$$\frac{\partial^2\phi}{\partial r^2} + \frac{1}{r}\frac{\partial\phi}{\partial r} + \frac{\partial^2\phi}{\partial z^2} = 0, \quad \frac{\partial T}{\partial t} + \frac{\partial\phi}{\partial r}\frac{\partial T}{\partial r} + \frac{\partial\phi}{\partial z}\frac{\partial T}{\partial z} = \frac{k}{\rho c}\left\{\frac{\partial^2 T}{\partial r^2} + \frac{1}{r}\frac{\partial T}{\partial r} + \frac{\partial^2 T}{\partial z^2}\right\} \quad \text{for } \eta(r,t) < z < h(r,t), \tag{11}$$

$$\frac{\partial T}{\partial t} = \frac{k}{\rho c}\left\{\frac{\partial^2 T}{\partial r^2} + \frac{1}{r}\frac{\partial T}{\partial r} + \frac{\partial^2 T}{\partial z^2}\right\} \quad \text{for } z < \eta(r,t), \tag{12}$$

$$T = V, \quad \frac{\partial\phi}{\partial t} + \frac{1}{2}\left(\left(\frac{\partial\phi}{\partial r}\right)^2 + \left(\frac{\partial\phi}{\partial z}\right)^2\right) + \frac{p}{\rho} = 0 \text{ on } z = h(r,t), \tag{13}$$

$$-I + k\left(\frac{\partial T}{\partial z} - \frac{\partial h}{\partial r}\frac{\partial T}{\partial r}\right) + \rho L_v\left(-\frac{\partial h}{\partial t} - \frac{\partial h}{\partial r}\frac{\partial\phi}{\partial r} + \frac{\partial\phi}{\partial z}\right) = 0 \text{ on } z = h(r,t), \tag{14}$$

$$T = T_m, \quad \frac{\partial\phi}{\partial z} = \frac{\partial\eta}{\partial r}\frac{\partial\phi}{\partial r}, \quad \rho L_f\frac{\partial\eta}{\partial t} + k\left[\frac{\partial T}{\partial z} - \frac{\partial\eta}{\partial r}\frac{\partial T}{\partial r}\right]_{\eta^-}^{\eta^+} = 0 \text{ on } z = \eta(r,t), \tag{15}$$

$$T \to T_a \quad \text{as } z \to -\infty, \tag{16}$$

where p is the recoil pressure, I is the input of laser energy, $V(p)$ is the vaporisation temperature as a function of recoil pressure and $L_v(V)$ is the latent heat of vaporisation. The first boundary condition in (13) is the vaporisation isotherm and the second conservation of momentum. Boundary condition (14) represents

conservation of energy. The first boundary condition in (15) is the melting isotherm, the second conservation of mass and the third conservation of energy.

The recoil pressure, the input of laser energy and the vaporisation temperature are required to complete the mathematical model for splashing. Ideally these quantities could be obtained from a numerical simulation of the axisymmetric domain above the fluid, but this is computationally expensive. An alternative approach, which involves modelling the domain as an infinite set of one-dimensional problems, is outlined in the Appendix.

We transform to dimensionless variables via $\phi = UL\hat{\phi}$, $T = T_m + (T_v - T_m)\hat{T}$, $\eta = d\hat{\eta}$, $h = d\hat{h}$, $r = L\hat{r}$, $z = d\hat{z}$ and $t = L\hat{t}/U$. The axisymmetric splashing model then becomes (and without ambiguity the hats on the non-dimensional variables can be omitted)

$$\frac{\partial^2\phi}{\partial r^2}+\frac{1}{r}\frac{\partial\phi}{\partial r}+\frac{1}{\delta^2}\frac{\partial^2\phi}{\partial z^2}=0,\quad \frac{\partial T}{\partial t}+\frac{\partial\phi}{\partial r}\frac{\partial T}{\partial r}+\frac{1}{\delta^2}\frac{\partial\phi}{\partial z}\frac{\partial T}{\partial z}=D\left\{\delta^2\left(\frac{\partial^2 T}{\partial r^2}+\frac{1}{r}\frac{\partial T}{\partial r}\right)+\frac{\partial^2 T}{\partial z^2}\right\}\ \text{for}\ \eta(r,t)<z<h(r,t), \tag{17}$$

$$\frac{\partial T}{\partial t}=D\left\{\delta^2\left(\frac{\partial^2 T}{\partial r^2}+\frac{1}{r}\frac{\partial T}{\partial r}\right)+\frac{\partial^2 T}{\partial z^2}\right\}\ \text{for}\ z<\eta(r,t), \tag{18}$$

$$T=\bar{V},\ \frac{\partial\phi}{\partial t}+\frac{1}{2}\left(\frac{\partial\phi}{\partial r}\right)^2+\frac{1}{2\delta^2}\left(\frac{\partial\phi}{\partial z}\right)^2+\bar{p}=0, \tag{19}$$

$$\frac{1}{\delta^2}\frac{\partial\phi}{\partial z}-\frac{\partial\phi}{\partial r}\frac{\partial h}{\partial r}-\frac{\partial h}{\partial t}=\bar{I}-\frac{D}{\lambda_v\bar{L}_v}\left(\frac{\partial T}{\partial z}-\delta^2\frac{\partial h}{\partial r}\frac{\partial T}{\partial r}\right)\ \text{on}\ z=h(r,t), \tag{20}$$

$$T=0,\ \frac{1}{\delta^2}\frac{\partial\phi}{\partial z}=\frac{\partial\phi}{\partial r}\frac{\partial\eta}{\partial r},\ \lambda_f\frac{\partial\eta}{\partial t}+D\left[\frac{\partial T}{\partial z}-\delta^2\frac{\partial\eta}{\partial r}\frac{\partial T}{\partial r}\right]_{\eta^-}^{\eta^+}=0\ \text{on}\ z=\eta(r,t), \tag{21}$$

$$T\to\bar{T}_a\quad\text{as}\quad z\to-\infty, \tag{22}$$

where $\bar{V}=(V(p)-T_m)/(T_v-T_m)$, $\bar{p}=p/\rho U^2$, $\bar{I}=IL/\rho dUL_v$ (where typically $\bar{I}\sim 0.1$) and $\bar{L}_v=L_v/L_v(T_v)$ are specified functions. The dimensionless constants δ, D, λ_f, λ_v and $\bar{T}_a$ are defined, and typical values given in Table 2; the constraints $\delta^2 \ll 1$ and $1/\lambda_v \ll 1$ typically hold in practice. The model is regularly perturbed in these small parameters. The parameter λ_v represents the Stefan number for vaporisation.

3 The leading-order problem

3.1 Solidification model

3.1.1 Asymptotic analysis

We now derive the leading-order equations for the solidification model. We introduce expansions of the form

$$\phi\sim\phi_0+\delta^2\phi_1,\quad T\sim T_0+\delta^2 T_1,\quad h\sim h_0+\delta^2 h_1,\quad \eta\sim\eta_0+\delta^2\eta_1.$$

We transfer the condition from the correct boundary $y=\eta$ to a convenient boundary $y=\eta_0$ by using a Taylor series expansion, that is

$$\left.\frac{\partial\phi}{\partial y}\right|_{y=\eta}=\left.\frac{\partial\phi_0}{\partial y}\right|_{y=\eta_0}+\delta^2\left(\left.\frac{\partial\phi_1}{\partial y}\right|_{y=\eta_0}+\eta_1\left.\frac{\partial^2\phi_0}{\partial y^2}\right|_{y=\eta_0}\right)+O(\delta^4).$$

A similar transfer takes place between $y=h$ and $y=h_0$. From the first equation in (6) and the second boundary condition in (9) we obtain

$$\phi\sim a+\delta^2\left\{b-\frac{a_{xx}y^2}{2}+(a_x\eta_0)_x y\right\} \tag{23}$$

where $a = a(x,t)$ and $b = b(x,t)$ are unknown functions. Substituting (23) into the second equation in (6), the first boundary condition in (8) and the second boundary condition in (8) gives

$$\frac{\partial T_0}{\partial t} + a_x \frac{\partial T_0}{\partial x} + \{(a_x \eta_0)_x - a_{xx} y\} \frac{\partial T_0}{\partial y} = D \frac{\partial^2 T_0}{\partial y^2}, \quad \frac{\partial h_0}{\partial t} + \frac{\partial}{\partial x}\{a_x (h_0 - \eta_0)\} = 0, \quad a_t + \frac{(a_x)^2}{2} = 0,$$

respectively. Finally, we make the substitution $u = a_x$ to give a differential equation for the temperature

$$\frac{\partial T_0}{\partial t} + u \frac{\partial T_0}{\partial x} + \{(u\eta_0)_x - u_x y\} \frac{\partial T_0}{\partial y} = D \frac{\partial^2 T_0}{\partial y^2} \quad \text{for} \quad \eta_0 < y < h_0, \tag{24}$$

with two boundary conditions

$$\text{on} \quad y = \eta_0 \quad T_0 = 0, \quad \text{on} \quad y = h_0 \quad \frac{\partial T_0}{\partial y} = 0, \tag{25}$$

the equation for the evolution of the velocity

$$u_t + u u_x = 0, \tag{26}$$

the equations for the evolution of the free boundaries

$$\frac{\partial h_0}{\partial t} + \frac{\partial}{\partial x}\{u(h_0 - \eta_0)\} = 0, \quad \lambda_f \frac{\partial \eta_0}{\partial t} + D \left[\frac{\partial T_0}{\partial y}\right]_{\eta_0^-}^{\eta_0^+} = 0, \tag{27}$$

the equation and the boundary condition for conduction in the solid

$$\frac{\partial T_0}{\partial t} = D \frac{\partial^2 T_0}{\partial y^2} \quad \text{for} \quad y < \eta_0 \quad \text{and} \quad T_0 \to \bar{T}_a \quad \text{as} \quad y \to -\infty. \tag{28}$$

The leading-order equations to describe solidification are (24)-(28). These equations are a combination of the shallow water equations and a two-phase Stefan problem. The appearance of the thermal convection in the vertical direction in the leading-order equations is due to the large vertical thermal gradients balancing with small vertical velocities. We note that this model only has a three-dimensional parameter space.

3.1.2 Shocks

We note that (26) uncouples from the system of equations (24)-(28). Let $u(x,0) = \tilde{u}(x)$ describe the initial velocity distribution, then $u(x,t)$ is given implicitly by $u = \tilde{u}(x - ut)$. Moreover, the slope is given by

$$u_x = \frac{\tilde{u}'(X)}{1 + t\tilde{u}'(X)}, \quad X = x - ut.$$

We have the following cases (i) $\tilde{u}'(X) \geq 0$ for all X so that no shocks develop or (ii) a shock will develop after a time given by $-1/\tilde{u}'(X_s)$ where X_s is the value of steepest negative slope. Case (ii) occurs in practice because the melt will always have compact support.

In the case of shocks it is necessary to obtain Rankine-Hugoniot conditions for the full system of equations. We need to rewrite (24), (26) and the first equation in (27) in conservation form

$$\frac{\partial}{\partial t}(h_0 - \eta_0) + \frac{\partial}{\partial x}(u(h_0 - \eta_0)) = -\frac{\partial \eta_0}{\partial t}, \tag{29}$$

$$\frac{\partial}{\partial t}(u(h_0 - \eta_0)) + \frac{\partial}{\partial x}(u^2(h_0 - \eta_0)) = -u\frac{\partial \eta_0}{\partial t}, \tag{30}$$

$$\frac{\partial T_0}{\partial t} + \frac{\partial}{\partial x}(uT_0) + \frac{\partial}{\partial y}\left(\{(u\eta_0)_x - u_x y\} T_0 - D\frac{\partial T_0}{\partial y}\right) = 0. \tag{31}$$

Equation (29) is conservation of mass, (30) is conservation of momentum and (31) is conservation of energy. We neglect kinetic energy in (31) because $U^2/cT_m \ll 1$. The corresponding Rankine-Hugoniot conditions are $[h_0 - \eta_0]Q = [u(h_0 - \eta_0)]$, $[u(h_0 - \eta_0)]Q = [u^2(h_0 - \eta_0)]$ and $[T_0]Q = [uT_0]$ where square brackets denote the difference between the values of the quantity on the two sides of the shock and Q is the speed of the shock. The Rankine-Hugoniot condition for conservation of energy represents an infinite set of conditions parameterised by y.

The leading edge of the melt (of finite extent) will always be a shock. However, there is no mass flux through this leading-edge shock. The accumulation of solidified material (recast) is considered to be related to shocks behind which melt can amass.

3.1.3 Summary of the leading-order solidification problem

The conservative form of the equations in the fluid (29)- (31) indicate that a more natural choice of dependent variable is the film thickness $H = h_0 - \eta_0$ rather than h_0. We also replace T_0 and η_0 by θ and ψ to avoid complications with subscripts in subsequent asymptotic expansions. A simpler form of the system of equations suitable for numerical solution is given by

$$\frac{\partial H}{\partial t} + \frac{\partial}{\partial x}(uH) = -\frac{\partial \psi}{\partial t}, \qquad \frac{\partial}{\partial t}(uH) + \frac{\partial}{\partial x}(u^2 H) = -u\frac{\partial \psi}{\partial t}, \tag{32}$$

$$\frac{\partial \theta}{\partial t} + \frac{\partial}{\partial x}(u\theta) + \frac{\partial}{\partial y}\left(\{(u\psi)_x - u_x y\}\,\theta - D\frac{\partial \theta}{\partial y}\right) = 0, \quad \text{on} \quad y = \psi + H \quad \frac{\partial \theta}{\partial y} = 0, \tag{33}$$

in the fluid,

$$\lambda_f \frac{\partial \psi}{\partial t} + D\left[\frac{\partial \theta}{\partial y}\right]_{\psi^-}^{\psi^+} = 0, \quad \text{on} \quad y = \psi \quad \theta = 0, \tag{34}$$

at the interface and

$$\frac{\partial \theta}{\partial t} = D\frac{\partial^2 \theta}{\partial y^2} \quad \text{for} \quad y < \psi \quad \text{and} \quad \theta \to \bar{T}_a \quad \text{as} \quad y \to -\infty, \tag{35}$$

in the solid. The initial conditions are

$$u(x,0) = \tilde{u}(x), \qquad \theta(x,y,0) = \tilde{\theta}(x,y), \qquad H(x,0) = \tilde{H}(x), \qquad \psi(x,0) = 0. \tag{36}$$

where we assume $\tilde{\theta}(x,y) = \bar{T}_a$ for $y < 0$, and $\tilde{\theta}(x,0) = 0$ and $\partial\tilde{\theta}/\partial y(x,\tilde{H}(x)) = 0$ for $\tilde{H}(x) > 0$. The Rankine-Hugoniot conditions are given by

$$[H]Q = [uH], \qquad [uH]Q = [u^2 H], \qquad [\theta]Q = [u\theta]. \tag{37}$$

We note that the right-hand side of the equation for conservation of mass is the rate at which the material is solidified. Similar comments apply to the equation for conservation of momentum. Equations (32) are valid for plug flow independent of the irrotational assumptions which were required to construct the model in Subsection 2.2. The only term in which the form of the potential remains is the vertical convection of energy in (33); this term being essential to guarantee the appropriate enthalpy flux at $y = \psi$ and $y = \psi + H$.

3.2 Splashing model

We now summarise the splashing model in conservative form. We define the leading-order quantity u to be the radial velocity, θ the temperature, ψ the position of the fluid/solid boundary and H the film thickness. We obtain

$$\frac{\partial H}{\partial t} + \frac{1}{r}\frac{\partial}{\partial r}(ruH) = -\left(\bar{I} + \frac{\partial \psi}{\partial t}\right), \qquad \frac{\partial}{\partial t}(uH) + \frac{1}{r}\frac{\partial}{\partial r}(ru^2 H) = -u\left(\bar{I} + \frac{\partial \psi}{\partial t}\right) - H\frac{\partial \bar{p}}{\partial r}, \tag{38}$$

$$\frac{\partial\theta}{\partial t}+\frac{1}{r}\frac{\partial}{\partial r}(ru\theta)+\frac{\partial}{\partial z}\left(\left\{\frac{1}{r}\frac{\partial}{\partial r}(ru\psi)-\frac{z}{r}\frac{\partial}{\partial r}(ru)\right\}\theta-D\frac{\partial\theta}{\partial z}\right)=0,\quad \text{on}\quad z=\psi+H\quad \theta=\bar{V}, \tag{39}$$

in the fluid,

$$\lambda_f\frac{\partial\psi}{\partial t}+D\left[\frac{\partial\theta}{\partial z}\right]_{\psi-}^{\psi+}=0,\quad \text{on}\quad z=\psi\quad \theta=0, \tag{40}$$

at the interface and

$$\frac{\partial\theta}{\partial t}=D\frac{\partial^2\theta}{\partial z^2}\quad \text{for}\quad z<\psi\quad \text{and}\quad \theta\to\bar{T}_a\quad \text{as}\quad z\to-\infty, \tag{41}$$

in the solid. The initial conditions are

$$u(r,0)=0,\quad \theta(r,z,0)=\tilde{\theta}(r,z),\quad H(r,0)=\tilde{H}(r),\quad \psi(r,0)=0. \tag{42}$$

where we assume $\tilde{\theta}\to\bar{T}_a$ as $z\to-\infty$, and $\tilde{\theta}(r,0)=0$ and $\tilde{\theta}(r,\tilde{H})=\bar{V}$ for $\tilde{H}(r)>0$. The Rankine-Hugoniot conditions are identical to those for the solidification problem. We note that the right-hand side of the equation for conservation of mass represents solidification and evaporation. These effects are both present on the right-hand side of the conservation of momentum equation along with the radial pressure gradient term. Equations (38) are valid for plug flow independent of the irrotational assumptions. The previous comments concerning (33) may now be applied to (39).

4 Analytical solution of the solidification problem

4.1 The large-time limit: similarity transformation

We now consider self-similar solutions that occur whilst drilling deep holes ($\sim$ 10mm). We will assume the initial velocity distribution is such that there are no shocks apart from at the leading edge. After a long enough time the melt will spread out such that the solution is independent of the detailed structure of the initial conditions ($x\in[0,\infty)$). The solution of the problem is then self-similar with

$$T_0=\bar{T}(\zeta,\xi),\quad u=\bar{u}(\zeta),\quad \eta_0=t^{1/2}\bar{\eta}(\zeta),\quad h_0=t^{1/2}\bar{h}(\zeta)$$

where $\zeta=x/t$ and $\xi=y/\sqrt{t}$. Equations (24)-(28) transform to

$$(\bar{u}-\zeta)\frac{\partial\bar{T}}{\partial\zeta}+\left\{\frac{\mathrm{d}(\bar{u}\bar{\eta})}{\mathrm{d}\zeta}-\xi\left(\frac{1}{2}+\frac{\mathrm{d}\bar{u}}{\mathrm{d}\zeta}\right)\right\}\frac{\partial\bar{T}}{\partial\xi}=D\frac{\partial^2\bar{T}}{\partial\xi^2}\quad \text{for}\quad \bar{\eta}<\xi<\bar{h}, \tag{43}$$

$$-\zeta\frac{\partial\bar{T}}{\partial\zeta}-\frac{\xi}{2}\frac{\partial\bar{T}}{\partial\xi}=D\frac{\partial^2\bar{T}}{\partial\xi^2}\quad \text{for}\quad \xi<\bar{\eta}, \tag{44}$$

$$(\bar{u}-\zeta)\frac{\mathrm{d}\bar{u}}{\mathrm{d}\zeta}=0,\quad \frac{\bar{h}}{2}-\zeta\frac{\mathrm{d}\bar{h}}{\mathrm{d}\zeta}+\frac{\mathrm{d}(\bar{u}\bar{h})}{\mathrm{d}\zeta}=\frac{\mathrm{d}(\bar{u}\bar{\eta})}{\mathrm{d}\zeta},\quad \lambda_f\left(\frac{\bar{\eta}}{2}-\zeta\frac{\mathrm{d}\bar{\eta}}{\mathrm{d}\zeta}\right)+D\left[\frac{\partial\bar{T}}{\partial\xi}\right]_{\xi=\bar{\eta}^-}^{\xi=\bar{\eta}^+}=0, \tag{45}$$

$$\text{on}\quad \xi=\bar{\eta}\quad \bar{T}=0,\quad \text{on}\quad \xi=\bar{h}\quad \frac{\partial\bar{T}}{\partial\xi}=0,\quad \bar{T}\to\bar{T}_a\quad \text{as}\quad \xi\to-\infty. \tag{46}$$

We note that from the third equation in (45), the steady state of the solidification boundary satisfies the linear equation

$$\frac{\mathrm{d}\bar{\eta}}{\mathrm{d}\zeta}-\frac{\bar{\eta}}{2\zeta}=0$$

so that $\bar{\eta}=A\zeta^{1/2}$ and $\eta_0=Ax^{1/2}$ with A constant. The resolidified material grows parabolically along the side of the drilled wall. In the absence of shocks, other than the leading-edge shock, the resolidification will be in the form of thin layers.

The first equation in (45) implies that either $\bar{u} = \zeta$, $\bar{u}$ is a constant or a combination of these. The option adopted depending on the initial velocity distribution ($u(x,0) = \tilde{u}(x)$). If we select $\tilde{u}(0) = 0$ and $\tilde{u}'(x) > 0$ where $\bar{h} > \bar{\eta}$, then the large-time velocity will be of the form $\bar{u} = \zeta$ or $u = x/t$. We may now solve (43) subject to the first and second boundary conditions in (46) to obtain $\bar{T} = 0$ for $\bar{\eta} < \xi < \bar{h}$; the liquid being at the melting point. The system of equations reduces to (44) with the first and third boundary conditions in (46) along with

$$\frac{3\bar{h}}{2} = \frac{\mathrm{d}(\zeta\bar{\eta})}{\mathrm{d}\zeta}, \quad \lambda_f\left(\frac{\bar{\eta}}{2} - \zeta\frac{\mathrm{d}\bar{\eta}}{\mathrm{d}\zeta}\right) = D\left.\frac{\partial\bar{T}}{\partial\xi}\right|_{\xi=\bar{\eta}^-}. \tag{47}$$

The first equation in (47) uncouples and we do not consider it any further. Therefore, the resolidified boundary is independent of the fluid depth in this case. We make the transformation to the new independent variables $s = \xi - \bar{\eta}(\zeta)$ and $q = \ln(1/\zeta)$ to obtain

$$\frac{\partial\bar{T}}{\partial q} - \frac{\partial\bar{T}}{\partial s}\left(\frac{s}{2} + \frac{D}{\lambda_f}\left.\frac{\partial\bar{T}}{\partial s}\right|_{s=0^-}\right) = D\frac{\partial^2\bar{T}}{\partial s^2}, \tag{48}$$

subject to the boundary conditions

$$\text{on} \quad s = 0 \quad \bar{T} = 0, \quad \bar{T} \to \bar{T}_a \quad \text{as} \quad s \to -\infty, \tag{49}$$

and the initial condition $\bar{T}(s,0) = w(s)$, where $w(s)$ may only be determined numerically. Equation (48) is a nonlinear convection-diffusion equation.

4.2 Small diffusion

In this subsection we assume that $D \ll 1$ and a particular $\tilde{u}(x)$ which allows us to make analytical progress with the system of equations (32)-(36); the choice of initial velocity distribution being given by $\tilde{u}(x) = x$ for $0 \le x \le 1$ and $\tilde{u}(x) = 0$ otherwise. The model is singularly perturbed in the small parameter D. Small diffusion corresponds to the molten metal having a high velocity after the splash. The results in this section may be used to validate a numerical solution.

We introduce expansions of the form $u \sim u_0$, $\theta \sim \theta_0$, $H \sim H_0$ and $\psi \sim D^{1/2}\psi_0$. The following solutions are obtained in the fluid,

$$u_0 = \frac{x}{1+t}, \quad \theta_0 = \tilde{\theta}\left(\frac{x}{1+t}\,,\, y(1+t)\right), \quad H_0 = \frac{1}{1+t}\tilde{H}\left(\frac{x}{1+t}\right) \quad \text{for} \quad 0 \le x \le 1+t.$$

We note that θ_0 satisfies both the boundary conditions given by the second equation in (33) and the second equation in (34). Therefore there is no boundary layer in the fluid despite the removal of the highest derivative in the leading-order problem. In the solid there is an outer expansion and an inner expansion near $y = \psi$. The outer expansion is given by $\theta \sim \bar{T}_a$. We perform the stretching transformation $y = D^{1/2}Y$ in the boundary layer, to obtain the leading-order problem

$$\frac{\partial\theta_0}{\partial t} = \frac{\partial^2\theta_0}{\partial Y^2}, \quad \theta_0(x,\psi_0,t) = 0 \text{ for } t > t^*, \quad \theta_0 \to \bar{T}_a \text{ as } Y \to -\infty, \quad \theta_0(x,Y,t^*) = \bar{T}_a, \quad \lambda_f\frac{\partial\psi_0}{\partial t} = \left.\frac{\partial\theta_0}{\partial Y}\right|_{Y=\psi_0^-}$$

where $t^* = \max(x-1,0)$. We thus have

$$\theta_0 = \bar{T}_a - \frac{\bar{T}_a}{1+\mathrm{erf}(\bar{\psi}/2)}\left(1 + \mathrm{erf}\left(\frac{Y}{2\sqrt{t-\max(x-1,0)}}\right)\right) \quad \text{for} \quad t \ge \max(x-1,0)$$

where $\bar{\psi}$ is the unique root of the transcendental equation

$$\lambda_f\sqrt{\pi}\bar{\psi}\exp\left(\frac{\bar{\psi}^2}{4}\right)\left(1+\mathrm{erf}\left(\frac{\bar{\psi}}{2}\right)\right) = -2\bar{T}_a,$$

provided that $\bar{T}_a < \lambda_f$. Finally, $\psi_0 = \bar{\psi}\sqrt{t - \max(x-1, 0)}$. This is essentially the Neumann solution [13, p. 158]. The temperature in the fluid does not influence the leading-order term for solidification due to the absence of large temperature gradients. This solution on $t = O(1)$ is an inner solution which breaks down on the longer time-scale $t = O(D^{-1/3})$. A number of variables need to be rescaled in this outer region, that is $t = D^{-1/3}\bar{t}$, $x = D^{-1/3}\bar{x}$, $y = D^{1/3}\bar{y}$, $H = D^{1/3}\bar{H}$ and $\psi = D^{1/3}\bar{\psi}$. The leading-order problem on this longer time-scale corresponds to a complete balance and no further analytical progress is possible. We note that for deep holes and small diffusion, the thickness of the resolidified material is $O(D^{1/3})$ spread over a region $O(D^{-1/3})$.

5 Weak formulation

5.1 Introduction

Weak formulations have been studied widely in the context of the Stefan problem (see [3] and references therein). However, the Stefan problem in which the fluid is moving across a solid surface has received scant attention. The purpose of this section is to incorporate a weak formulation of the conservation of energy equation into our models for solidification and splashing. Moreover, we prove that solutions of the weak formulations include all classical solutions.

5.2 Solidification problem

We define $X_L(t)$ and $X_U(t)$ to be the points $X_L(t) = \inf\{x : H(x,t) > 0\}$ and $X_U(t) = \sup\{x : H(x,t) > 0\}$ (shown in Figure 2). We assume that the fluxes of mass, momentum and energy are zero at the limits of the fluid region, so that

$$\text{on } x = X_L(t)^-, X_U(t)^+ \text{ and } y = \psi \quad uH = u^2H = u\theta = 0. \tag{50}$$

If $u \geq 0$ then (50) on $x = X_L(t)^-$ are boundary conditions for (32)-(33); the case $u \leq 0$ being similar. Let $\Omega(t)$ be the region in $\mathbb{R}^2$ such that $X_L(t) < x < X_U(t)$ and $y < \psi + H$. For any $\tau > 0$, let $\Omega_\tau = \bigcup_{t<\tau} \Omega(t)$. We define

$$\begin{aligned} \Omega^+(t) &= \{(x,y) \in \Omega(t) : S(x,y,t) > 0 \text{ and } \theta > 0\} \text{ (liquid)}, \\ \Omega^-(t) &= \{(x,y) \in \Omega(t) : S(x,y,t) < 0 \text{ and } \theta < 0\} \text{ (solid)}, \end{aligned}$$

$$\Gamma = \{(x,y,t) \in \Omega_\tau : S(x,y,t) = 0\}, \quad \Omega_\tau^+ = \bigcup_{t<\tau} \Omega^+(t), \quad \Omega_\tau^- = \bigcup_{t<\tau} \Omega^-(t),$$

where $S(x,y,t) = y - \psi(x,t)$. We define the dimensionless enthalpy, E, by

$$E = \begin{cases} \theta & \theta < 0 \quad \text{(solid)}, \\ \theta + \lambda_f & \theta > 0 \quad \text{(liquid)}, \end{cases}$$

and therefore

$$\theta = \begin{cases} E & E < 0, \\ 0 & 0 < E < \lambda_f, \\ E - \lambda_f & E > \lambda_f, \end{cases} \tag{51}$$

The classical formulation of $(33)_1$ and $(35)_1$ may be written in the form

$$\frac{\partial E}{\partial t} + \frac{\partial}{\partial x}(\chi u\theta) + \frac{\partial}{\partial y}\left(\chi\left\{\frac{\partial}{\partial x}(u\psi) - \frac{\partial u}{\partial x}y\right\}\theta - D\frac{\partial \theta}{\partial y}\right) = 0 \text{ for } (x,y,t) \in \Omega_\tau \setminus \Gamma, \tag{52}$$

where χ is the Heaviside function

$$\chi = \begin{cases} 0 & \theta < 0 \quad \text{(solid)}, \\ 1 & \theta > 0 \quad \text{(liquid)}. \end{cases}$$

We define the functions $\{\theta,\ S\}$ to be a classical solution if

(A) θ, $\partial S/\partial t$ and $\boldsymbol{\nabla} S$ are continuous on Ω_τ,

(B) $\partial\theta/\partial t$, $\boldsymbol{\nabla}\theta$ and $\nabla^2\theta$ are continuous on $\Omega_\tau \setminus \Gamma$,

(C) (32), $(33)_2$, (34), $(35)_2$, (36), (50), (51) and (52) are satisfied.

We define a weak solution of the solidification model to be a pair of bounded integrable functions $\{\theta,\ E\}$ defined on Ω_τ such that (32), $(35)_2$, (36), (50) and (51) are satisfied and the integral identity

$$\int_{\Omega_\tau} \left(E\frac{\partial v}{\partial t} + \chi u\theta\frac{\partial v}{\partial x} + \chi\left\{\frac{\partial}{\partial x}(u\psi) - \frac{\partial u}{\partial x}y\right\}\theta\frac{\partial v}{\partial y} + D\theta\frac{\partial^2 v}{\partial y^2}\right) dydxdt$$

$$= -\int_{\Omega(0)} v(x,y,0)E(x,y,0)dydx + \int_{t=0}^{\tau}\int_{x=X_L(t)}^{X_U(t)} v(x,\psi+H,t)\lambda_f\frac{\partial}{\partial x}(uH)dxdt$$

$$+\int_{t=0}^{\tau}\int_{y=-\infty}^{\psi(X_L(t),t)} \frac{\mathrm{d}X_L}{\mathrm{d}t}v(X_L(t),y,t)\theta(X_L(t),y,t)dydt - \int_{t=0}^{\tau}\int_{y=-\infty}^{\psi(X_U(t),t)} \frac{\mathrm{d}X_U}{\mathrm{d}t}v(X_U(t),y,t)\theta(X_L(t),y,t)dydt \tag{53}$$

holds for all test functions $v \in \mathcal{F}$, where

$$\mathcal{F} = \left\{\phi \in C^1(\bar{\Omega}_\tau) : \frac{\partial^2\phi}{\partial x_i \partial x_j} \in C(\bar{\Omega}_\tau),\ \phi(x,y,\tau) = 0,\ \frac{\partial\phi}{\partial y}(x,\psi+H,t) = 0,\ \phi \to 0 \text{ as } y \to -\infty\right\}.$$

If θ were to be replaced by E in the convection terms in (52), that is

$$\frac{\partial E}{\partial t} + \frac{\partial}{\partial x}(\chi uE) + \frac{\partial}{\partial y}\left(\chi\left\{\frac{\partial}{\partial x}(u\psi) - \frac{\partial u}{\partial x}y\right\}E - D\frac{\partial\theta}{\partial y}\right) = 0 \text{ for } (x,y,t) \in \Omega_\tau \setminus \Gamma,$$

then the second term on the right-hand side of (53) would be removed. The formulation (52) is preferred because $\theta(x,\psi,t) = 0$ and θ is continuous whereas the enthalpy E is discontinuous at $y = \psi$ which may well increase discretisation errors. The most important implication of the weak formulation is that the discretisation of (32), $(33)_2$, $(35)_2$, (36), (50), (51) and (52) may converge to a weak solution as the mesh size tends to zero (a proof exists for the standard Stefan problem, see [3] and references therein). Further investigation of these conjectures is required along with the questions of existence, uniqueness and well-posedness.

Theorem 1

1. A classical solution is also a weak solution.
2. If $\{\theta,\ E\}$ is a weak solution and there is a function S such that (34), (A) and (B) hold, then $\{\theta,\ S\}$ is a classical solution.

Proof

1. Let $v \in \mathcal{F}$. If $\{\theta,\ S\}$ is a classical solution then

$$\begin{aligned} 0 &= \int_{\Omega_\tau^+} v\left(\frac{\partial E}{\partial t} + \frac{\partial}{\partial x}(\chi u\theta) + \frac{\partial}{\partial y}\left(\chi\left\{\frac{\partial}{\partial x}(u\psi) - \frac{\partial u}{\partial x}y\right\}\theta - D\frac{\partial\theta}{\partial y}\right)\right) dydxdt \\ &= -\int_{\Omega_\tau^+}\left(E\frac{\partial v}{\partial t} + \chi u\theta\frac{\partial v}{\partial x} + \chi\left\{\frac{\partial}{\partial x}(u\psi) - \frac{\partial u}{\partial x}y\right\}\theta\frac{\partial v}{\partial y} + D\theta\frac{\partial^2 v}{\partial y^2}\right) dydxdt \\ &\quad + \int_{\Omega_\tau^+}\frac{\partial}{\partial t}(vE) + \frac{\partial}{\partial x}(v\chi u\theta) + \frac{\partial}{\partial y}\left(v\chi\left\{\frac{\partial}{\partial x}(u\psi) - \frac{\partial u}{\partial x}y\right\}\theta - Dv\frac{\partial\theta}{\partial y} + D\theta\frac{\partial v}{\partial y}\right) dydxdt. \end{aligned}$$

Now, by the divergence theorem,

$$\begin{aligned} &\int_{\Omega_\tau^+}\left(E\frac{\partial v}{\partial t} + \chi u\theta\frac{\partial v}{\partial x} + \chi\left\{\frac{\partial}{\partial x}(u\psi) - \frac{\partial u}{\partial x}y\right\}\theta\frac{\partial v}{\partial y} + D\theta\frac{\partial^2 v}{\partial y^2}\right) dydxdt \\ &= \int_{\partial\Omega_\tau^+}\left(vE,\ v\chi u\theta,\ v\chi\left\{\frac{\partial}{\partial x}(u\psi) - \frac{\partial u}{\partial x}y\right\}\theta - Dv\frac{\partial\theta}{\partial y} + D\theta\frac{\partial v}{\partial y}\right)\cdot(n_t,\ n_x,\ n_y)dS \\ &= -\int_{\Omega^+(0)} v(x,y,0)E(x,y,0)dydx + \int_{t=0}^{\tau}\int_{x=X_L(t)}^{X_U(t)} v(x,\psi+H,t)\lambda_f\frac{\partial}{\partial x}(uH)dxdt \\ &\qquad + \int_\Gamma v\left(E\frac{\partial\psi}{\partial t} + D\frac{\partial\theta}{\partial y}\right)\frac{dS}{|n|}, \end{aligned} \tag{54}$$

where $|n|^2 = (\partial\psi/\partial t)^2 + (\partial\psi/\partial x)^2 + 1$. We have used the final condition on v, the boundary conditions for $\partial\psi/\partial y$ and $\partial v/\partial y$ on $y = \psi + H$ and the boundary conditions for θ on $y = \psi$. Similarly for Ω_τ^-, we obtain

$$\begin{aligned} &\int_{\Omega_\tau^-}\left(E\frac{\partial v}{\partial t} + \chi u\theta\frac{\partial v}{\partial x} + \chi\left\{\frac{\partial}{\partial x}(u\psi) - \frac{\partial u}{\partial x}y\right\}\theta\frac{\partial v}{\partial y} + D\theta\frac{\partial^2 v}{\partial y^2}\right) dydxdt \\ &= -\int_{\Omega^-(0)} v(x,y,0)E(x,y,0)dydx - \int_\Gamma v\left(E\frac{\partial\psi}{\partial t} + D\frac{\partial\theta}{\partial y}\right)\frac{dS}{|n|} \\ &+ \int_{t=0}^{\tau}\int_{y=-\infty}^{\psi(X_L(t),t)}\frac{\mathrm{d}X_L}{\mathrm{d}t}v(X_L(t),y,t)\theta(X_L(t),y,t)dydt \\ &- \int_{t=0}^{\tau}\int_{y=-\infty}^{\psi(X_U(t),t)}\frac{\mathrm{d}X_U}{\mathrm{d}t}v(X_U(t),y,t)\theta(X_L(t),y,t)dydt. \end{aligned} \tag{55}$$

The third term on the right-hand side of (54) and the second term on the right-hand side of (55) cancel due to $(34)_1$, therefore the classical solution satisfies (53).

2. Let $v \in C_0^\infty(\Omega_\tau^+)$. Then, substituting into (53),

$$\begin{aligned} 0 &= \int_{\Omega_\tau^+}\left(E\frac{\partial v}{\partial t} + \chi u\theta\frac{\partial v}{\partial x} + \chi\left\{\frac{\partial}{\partial x}(u\psi) - \frac{\partial u}{\partial x}y\right\}\theta\frac{\partial v}{\partial y} + D\theta\frac{\partial^2 v}{\partial y^2}\right) dydxdt \\ &= -\int_{\Omega_\tau^+} v\left(\frac{\partial E}{\partial t} + \frac{\partial}{\partial x}(\chi u\theta) + \frac{\partial}{\partial y}\left(\chi\left\{\frac{\partial}{\partial x}(u\psi) - \frac{\partial u}{\partial x}y\right\}\theta - D\frac{\partial\theta}{\partial y}\right)\right) dydxdt. \end{aligned}$$

Since θ is smooth, we have (52) in Ω_τ^+ and the same argument holds for Ω_τ^-. The boundary condition $(33)_2$ and Stefan condition $(34)_1$ are obtained by taking test functions whose supports are neighbourhoods of the surfaces $y - \psi - H = 0$ and Γ, respectively.

5.3 Splashing problem

We define $R_U(t)$ to be $R_U(t) = \sup\{r : H(r,t) > 0\}$ (shown in Figure 3). We assume that the fluxes of mass, momentum and energy are zero at the limit of the fluid region, so that

$$\text{on } r = R_U(t)^+ \text{ and } z = \psi \quad uH = u^2H = u\theta = 0. \tag{56}$$

Let $\Omega(t)$ be the region in $\mathbb{R}^2$ such that $0 < r < R_U(t)$ and $z < \psi + H$. For any $\tau > 0$, let $\Omega_\tau = \bigcup_{t<\tau} \Omega(t)$. We again define $\Gamma = \{(r,z,t) \in \Omega_\tau : S(r,z,t) = 0\}$ where $S(r,z,t) = z - \psi(r,t)$. The classical formulation of $(39)_1$ and $(41)_1$ may be written in the form

$$\frac{\partial E}{\partial t} + \frac{1}{r}\frac{\partial}{\partial r}(\chi r u\theta) + \frac{\partial}{\partial z}\left(\chi\left\{\frac{1}{r}\frac{\partial}{\partial r}(ru\psi) - \frac{z}{r}\frac{\partial}{\partial r}(ru)\right\}\theta - D\frac{\partial\theta}{\partial z}\right) = 0 \text{ for } (r,z,t) \in \Omega_\tau \setminus \Gamma. \tag{57}$$

We define the functions $\{\theta,\ S\}$ to be a classical solution if (A) and (B) hold and

(D) (38), $(39)_2$, (40), $(41)_2$, (42), (51), (56) and (57) are satisfied.

We now define a weak solution of the splashing model to be a pair of bounded integrable functions $\{\theta,\ E\}$ defined on Ω_τ such that (38), $(41)_2$, (42), (51) and (56) are satisfied and the integral identity

$$\int_{\Omega_\tau} E\frac{\partial v}{\partial t} + \chi u\theta\frac{\partial v}{\partial r} + \chi\left\{\frac{1}{r}\frac{\partial}{\partial r}(ru\psi) - \frac{z}{r}\frac{\partial}{\partial r}(ru)\right\}\theta\frac{\partial v}{\partial z} + D\theta\frac{\partial^2 v}{\partial z^2} r dt dr dz$$

$$= -\int_{\Omega(0)} v(r,z,0)E(r,z,0) r dr dz + \int_{t=0}^{\tau}\int_{r=0}^{R_U(t)} \frac{\partial v}{\partial z}(r,\psi+H,t) D\bar{V} r dr dt$$

$$-\int_{t=0}^{\tau}\int_{z=-\infty}^{\psi(R_U(t),t)} \frac{\mathrm{d}R_U}{\mathrm{d}t} v(R_U(t),z,t)\theta(R_U(t),z,t) dz dt - \int_{t=0}^{\tau}\int_{z=\psi(0,t)}^{\psi(0,t)+H(0,t)} u(0,t)v(0,z,t)\theta(0,z,t) dz dt \tag{58}$$

holds for all test functions $v \in \mathcal{F}$, where

$$\mathcal{F} = \left\{\phi \in C^1(\bar{\Omega}_\tau) : \frac{\partial^2\phi}{\partial x_i \partial x_j} \in C(\bar{\Omega}_\tau),\ \phi(r,z,\tau) = 0,\ \phi(r,\psi+H,t) = 0,\ \phi \to 0 \text{ as } z \to -\infty\right\}.$$

Theorem 2

1. A classical solution is also a weak solution.
2. If $\{\theta,\ E\}$ is a weak solution and there is a function S such that (40), (A) and (B) hold, then $\{\theta,\ S\}$ is a classical solution.

The proof is similar to the proof of Theorem 1. The discretisation of (38), $(39)_2$, $(41)_2$, (42), (51), (56) and (57) should be studied for the splashing model.

6 Summary

Three mathematical models have been introduced to describe solidification and splashing in laser percussion drilling. The physical problem is turbulent flow between two unknown moving boundaries. In order to make the problem more tractable the following assumptions are made concerning the fluid flow (i) incompressible, (ii) axisymmetric, (iii) inviscid and (iv) negligible surface tension and gravity. The flow is also taken to be laminar and irrotational in the first model. This first model for laminar and irrotational flow is employed to derive a second averaged model. The second model is proposed for the turbulent flow.

The second model is derived from the first in the limit of small aspect ratio and large Stefan number for vaporisation. The resulting model is a combination of the shallow water equations and a two-phase Stefan problem. Shocks may occur. The accumulation of solidified material (recast) is considered to be related to shocks behind which the melt can amass. Therefore shocks are highly undesirable and may be avoided by ensuring that the melt velocity after the splash increases montonically from the centre of the hole, that is the radial pressure gradients should become steeper towards the perimeter of the hole. This must be achieved by accurate control of the radial laser intensity profile. In the absence of shocks, other than the leading-edge shock, the resolidification will be in the form of thin layers. For deep holes these thin layers are found to grow parabolically. A key parameter group in the growth of the solidification is given by

$$\left(\frac{k}{\rho c}\right)^{1/2} \frac{c(T_m - T_a)}{L_f}.$$

As the material properties are usually fixed this highlights the importance of the difference between the melting and ambient temperatures and suggests experiments in which the metal target is heated prior to drilling. A heated target should suffer less from recast. Although heating may not be practical in commercial situations, reducing the time between pulses would have a similar effect.

A word of caution concerns the use of high laser intensity, in this régime only evaporation will take place. The resulting vapour will shield the metal surface by absorbing the laser radiation. A further word of caution regarding the use of high laser intensity concerns the increased probability of crack formation.

The last model modifies the second model by replacing the classical formulation of the energy equation with a weak formulation valid throughout the fluid, solid and at the fluid/solid interface. The convection terms in the energy equation for the fluid are unusual in this context. The weak formulation is far more amenable to numerical methods than the model in [6, 7] and is the first stage towards numerical calculations with the enthalpy method.

Acknowledgement

Financial support for this work was provided by the TMR contract entitled 'Differential Equations in Industry and Commerce'. This project has benefited from the generous advice of J. C. J. Verhoeven, J. K. M. Jansen, R. M. M. Mattheij and M. E. H. van Dongen.

References

[1] M. Allmen and A. Blatter, *Laser-Beam Interactions with Materials*, Springer-Verlag, Berlin, 1995.

[2] J. Dowden, M. Davis, and P. Kapadia, *Some aspects of fluid mechanics of laser welding*, J. Fluid Mech., 126 (1983), pp. 123–146.

[3] C. M. Elliott and J. R. Ockendon, *Weak and Variational Methods for Moving Boundary Problems*, Pitman Books Limited, London, 1982.

[4] A. C. Fowler, *Mathematical Models in the Applied Sciences*, Cambridge University Press, New York, 1997.

[5] M. C. Fowler and D. C. Smith, *Ignition and maintenance of subsonic plasma waves in atmospheric pressure air by cw CO_2 laser radiation and their effect on laser beam propagation*, J. Appl. Phys., 46 (1975), pp. 138–150.

[6] R. K. GANESH AND A. FAGHRI, *A generalized thermal modeling for laser drilling process–I. mathematical modeling and numerical methodology*, Int. J. Heat Mass Transfer, 40 (1997), pp. 3351–3360.

[7] ——, *A generalized thermal modeling for laser drilling process–II. numerical simulation and results*, Int. J. Heat Mass Transfer, 40 (1997), pp. 3361–3373.

[8] C. J. KNIGHT, *Theoretical modeling of rapid surface vaporization with back pressure*, AIAA J., 17 (1979), pp. 519–523.

[9] L. D. LANDAU AND E. M. LIFSCHITZ, *Statistical Mechanics*, Pergamon, New York, 1980.

[10] H. W. LIEPMANN AND A. ROSHKO, *Elements of Gas Dynamics*, John Wiley & Sons, New York, 1960.

[11] H. OCKENDON AND A. B. TAYLER, *Inviscid Fluid Flows*, Springer-Verlag, New York, 1983.

[12] K. RAŽNJEVIĆ, *Handbook of Thermodynamic Tables and Charts*, Hemisphere, London, 1976.

[13] A. B. TAYLER, *Mathematical Models in Applied Mechanics*, Oxford University Press, Oxford, 1986.

Appendix Gas Dynamics

The melt is ejected from the drilled hole by the radial pressure gradients generated by the sudden expansion of the vapour evaporating from the melt surface. The high recoil pressures involved also cause significant variation in the vaporisation temperature and rapid flow of vapour and air away from the melt surface. The following assumptions will be made (i) the time-scale of the gas dynamics is much smaller than the time-scale of the intensity variations, (ii) any beam/vapour interaction is negligible (the absorption coefficient of aluminium vapour is 0.5cm^{-1} at a temperature of 5000K [5] and a coaxial jet is employed to remove the aluminium vapour from the laser path), (iii) the vapour and air behave as ideal gases, (iv) there is no mixing between the aluminium vapour and compressed air, (v) the liquid-vapour interface has negligible width, (vi) all the laser energy is used to vaporise the melt, (vii) the three-dimensional problem can be viewed as an infinite set of one-dimensional problems parameterised by the intensity and (viii) the compression waves have coalesced to form discontinuities leaving the vapour and compressed air at constant pressure [10].

A schematic representation of the physical situation is shown in Figure 4, in which there are four regions [8]. The four regions are the ambient air, the compressed air, the metal vapour and the molten metal. These regions are separated by three interfaces: a shock between the ambient air ① and the compressed air ②, a contact surface between the compressed air ② and the metal vapour ③, and the liquid-vapour interface between the metal vapour ③ and the molten metal ④. Across the shock we have the Rankine-Hugoniot relations (see [11, p. 83])

$$\rho_1(U-u_1) = \rho_2(U-u_2), \tag{59}$$

$$p_1+\rho_1(U-u_1)^2 = p_2+\rho_2(U-u_2)^2, \tag{60}$$

$$c_1T_1+\frac{1}{2}(U-u_1)^2 = c_2T_2+\frac{1}{2}(U-u_2)^2, \tag{61}$$

where U is the shock speed, p the pressure, ρ the density, u the velocity, T the temperature, c the specific heat capacity at constant pressure and the subscripts denote the region of interest. Across the contact surface we have (see [10, p. 81])

$$p_2=p_3, \quad u_2=u_3. \tag{62}$$

Let L_v denote the latent heat of vaporisation, I the laser intensity and c_v the specific heat capacity at constant volume of the melt. Across the liquid-vapour interface we have

$$\rho_4 u_4 = \rho_3 u_3, \tag{63}$$

$$p_4 + \rho_4 u_4^2 = p_3 + \rho_3 u_3^2, \tag{64}$$

$$\rho_4 u_4 \left(c_v T_4 + \frac{1}{2} u_4^2 + \frac{p_4}{\rho_4} \right) + I = \rho_3 u_3 \left(c_3 T_3 + L_v + \frac{1}{2} u_3^2 \right), \tag{65}$$

representing conservation of mass, conservation of momentum and conservation of energy, respectively. We note that $\rho_3/\rho_4 \ll 1$, so that

$$u_4 \ll u_3, \quad \rho_4 u_4^2 \ll \rho_3 u_3^2, \quad \frac{1}{2} u_4^2 \ll \frac{1}{2} u_3^2, \quad \frac{p_4}{\rho_4} \ll \frac{p_3}{\rho_3}.$$

We now use our assumption that all the laser energy is used to vaporise the melt, to obtain

$$I = \rho_4 u_4 L_v.$$

We deduce the leading-order expressions for the liquid-vapour interface

$$\rho_3 u_3 = \frac{I}{L_v}, \quad p_3 + \rho_3 u_3^2 = p_4, \quad c_3 T_3 + \frac{1}{2} u_3^2 = c_v T_4. \tag{66}$$

We must add three constitutive laws to close the system of equations. The metal vapour and the compressed air have been assumed to be ideal gases, which yields

$$p_2 = R_2 \rho_2 T_2, \quad p_3 = R_3 \rho_3 T_3, \tag{67}$$

where R is the gas constant in the appropriate region. Across the liquid-vapour interface we use the Rankine-Kirchhoff equation

$$p_4(T_4) = p_4(T_{ref}) \left(\frac{T_4}{T_{ref}} \right)^{(c_3 - c_4)/R_3} \exp \left\{ \frac{L_0}{R_3} \left(\frac{1}{T_{ref}} - \frac{1}{T_4} \right) \right\}, \tag{68}$$

where the subscript ref corresponds to a reference state and $L_v = L_0 + (c_3 - c_4)T_4$. The Rankine-Kirchhoff equation is a first integral of the Clausius-Clapeyron equation [9]. The system to be solved consists of (59)-(62) and (66)-(68). The algebraic system of equations is solved with the routine C05NBF from the NAG library; the data being given in Table 3.

The recoil pressure as a function of intensity is shown in Figure 5. The radial pressure gradient can now be deduced from the known variation of intensity with radius. This is a necessary input to the splashing model. The high recoil pressure also causes the vaporisation temperature of the aluminium to vary considerably over this intensity régime (shown in Figure 6). This also has to serve as an input for the splashing model. In Figure 7 the different velocities as a function of intensity are sketched. The speed of sound in aluminium vapour is included to show that the compressed air speed or the speed of aluminium vapour is subsonic for the intensities of interest. This is in contrast to the assumptions in [6, 7]. The magnitude of these velocities with the typical length-scale ($\sim$ 1mm) allows us to determine the time-scale for the gas dynamics ($\sim 10^{-6}$s). The compressed air density is much larger than the density of the metal vapour (shown in Figure 8).

Symbol	Definition	Value
ρ	density	2.7×10^3 kg m $^{-3}$
$L_v(T_v)$	latent heat of vaporisation	1.2×10^7 J kg^{-1}
L_f	latent heat of fusion	3.6×10^5J kg^{-1}
k	thermal conductivity	2.3×10^2 W m^{-1}K^{-1}
c	specific heat capacity	9.0×10^2 J kg^{-1}K^{-1}
T_m	melting temperature	9.3×10^2K
T_v	vaporisation temperature	2.5×10^3 K
μ	viscosity	2.7×10^{-3} Pa s
σ	surface tension	1 kg s^{-2}

Table 1: Physical data for drilling aluminium

Symbol	Definition	Typical Value
δ	d/L	0.1
D	$k/\rho cUL\delta^2$	0.2
λ_f	$L_f/c(T_v - T_m)$	0.3
λ_v	$L_v(T_v)/c(T_v - T_m)$	8
$\bar{T}_a$	$(T_a - T_m)/(T_v - T_m)$	-0.4

Table 2: Dimensionless parameters for a typical laser percussion drilling process

Parameter	Value
R_1	3.0×10^2 N m kg^{-1} K^{-1}
R_2	3.0×10^2 N m kg^{-1} K^{-1}
R_3	3.1×10^2 N m kg^{-1} K^{-1}
c_1	1.0×10^3 J kg^{-1} K^{-1}
c_2	1.0×10^3 J kg^{-1} K^{-1}
c_3	5.0×10^2 J kg^{-1} K^{-1}
c_{p4}	1.0×10^3 J kg^{-1} K^{-1}
c_v	1.0×10^3 J kg^{-1} K^{-1}
$L_v(T_{ref})$	1.2×10^7 J kg^{-1}
T_{ref}	2.5×10^3 K
$p_4(T_{ref})$	1.2×10^5 N m^{-2}
u_1	0.0 m s^{-1}
p_1	1.0×10^5 N m^{-2}
T_1	3.0×10^2 K

Table 3: Physical data for aluminium vaporisation.

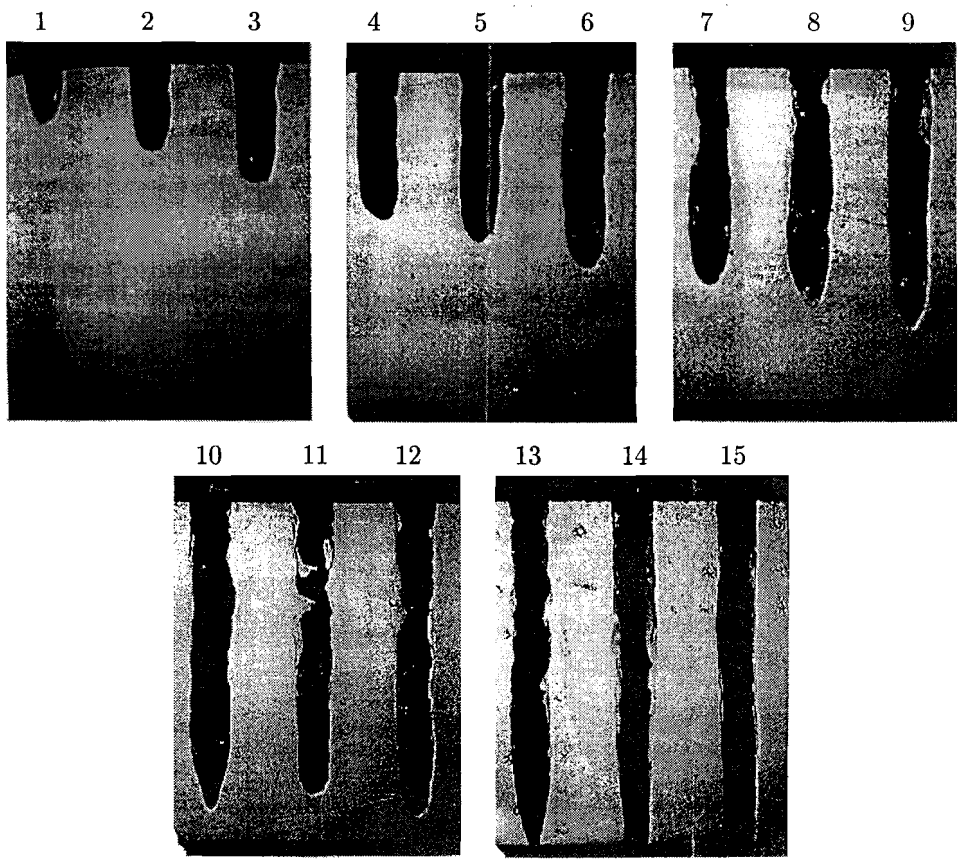

Figure 1: A series of photographs of holes produced by laser percussion drilling. The number of pulses to produce each hole is indicated (Courtesy of Eldim BV).

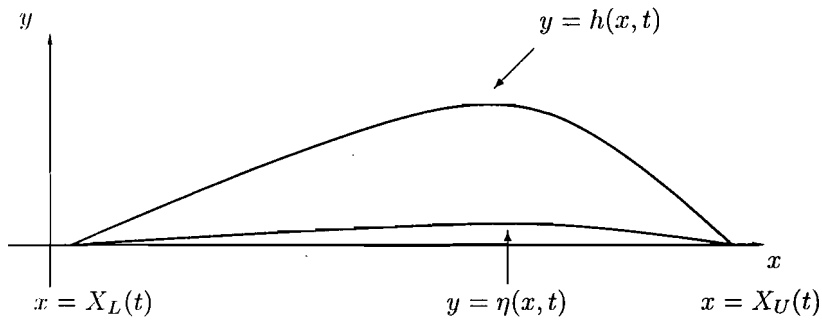

Figure 2: Planar representation of solidification. The horizontal direction is denoted by x and the vertical direction by y. The incompressible fluid is in the region $X_L(t) < x < X_U(t)$ and $\eta(x,t) < y < h(x,t)$, and the solid is in the region $y < \eta(x,t)$.

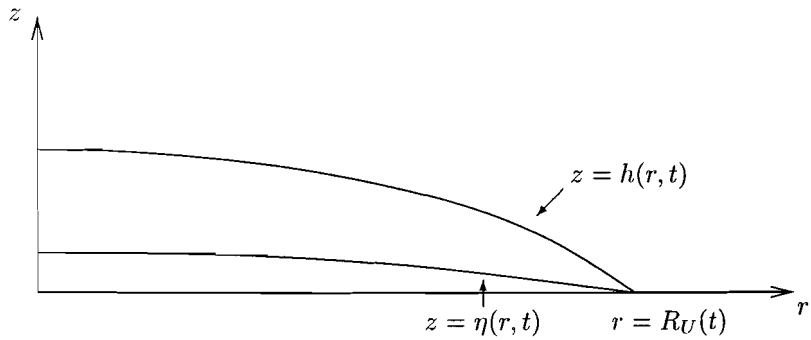

Figure 3: Axisymmetric representation of splashing. The axial direction is denoted by r and the vertical direction by z. The incompressible fluid is in the region $0 < r < R_U(t)$ and $\eta(r,t) < z < h(r,t)$, and the solid is in the region $z < \eta(r,t)$.

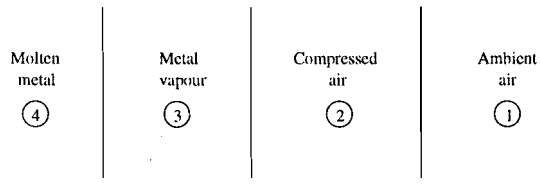

Figure 4: A schematic of the gas dynamics.

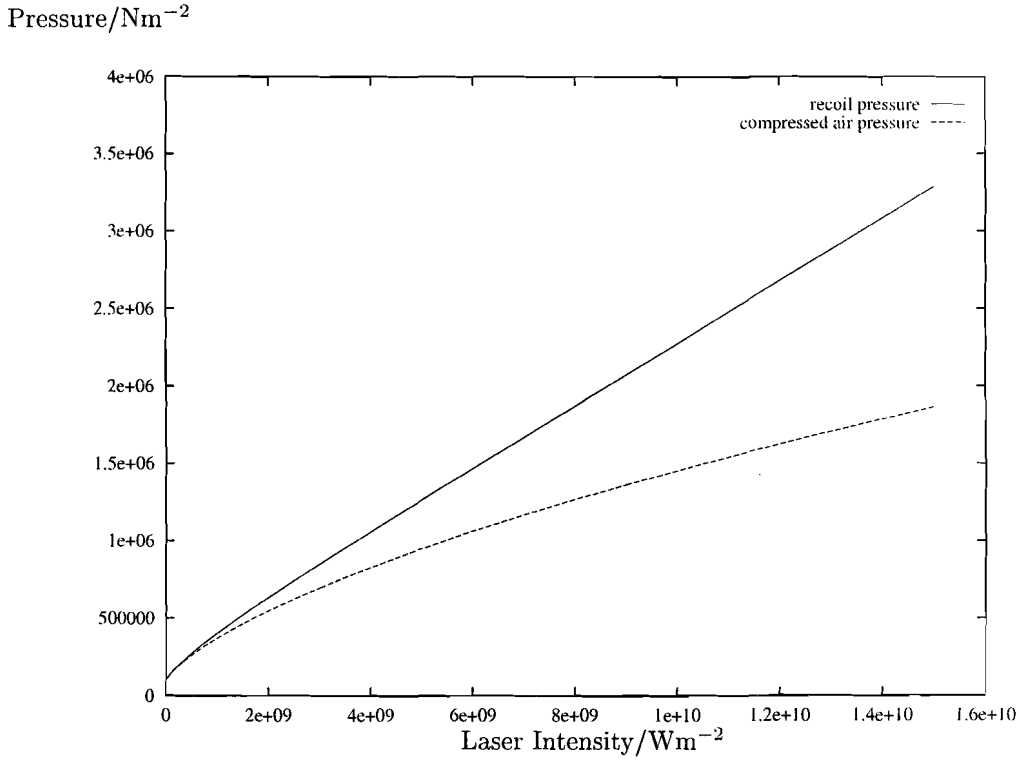

Figure 5: The recoil pressure and compressed air pressure as a function of laser intensity. The data is given in Table 3.

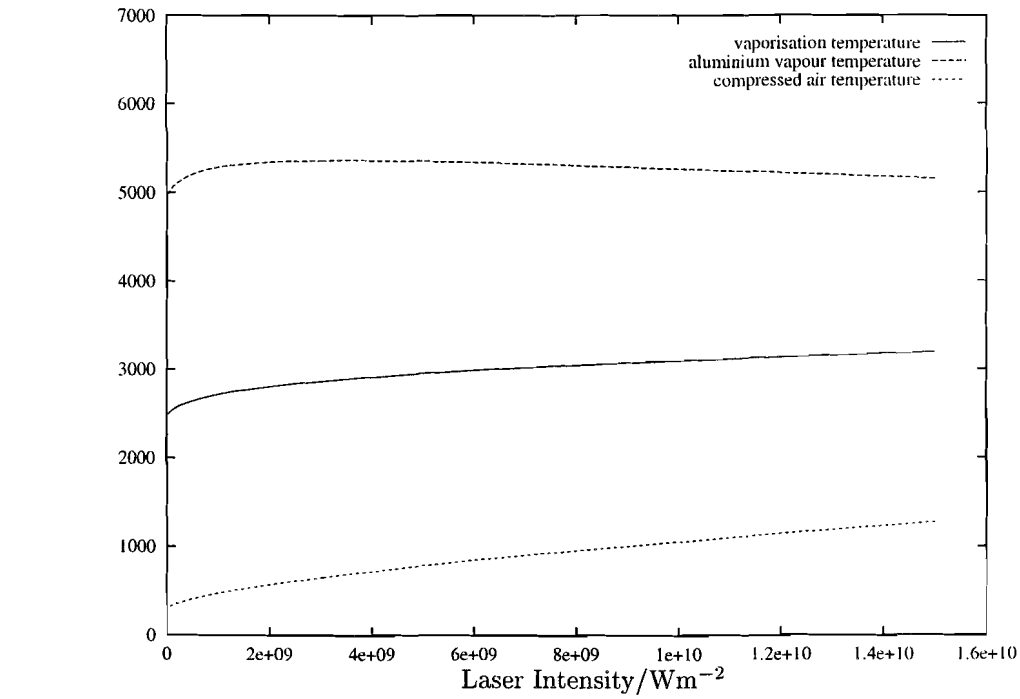

Figure 6: The vaporisation temperature, aluminium vapour temperature and compressed air temperature as a function of laser intensity. The data is given in Table 3.

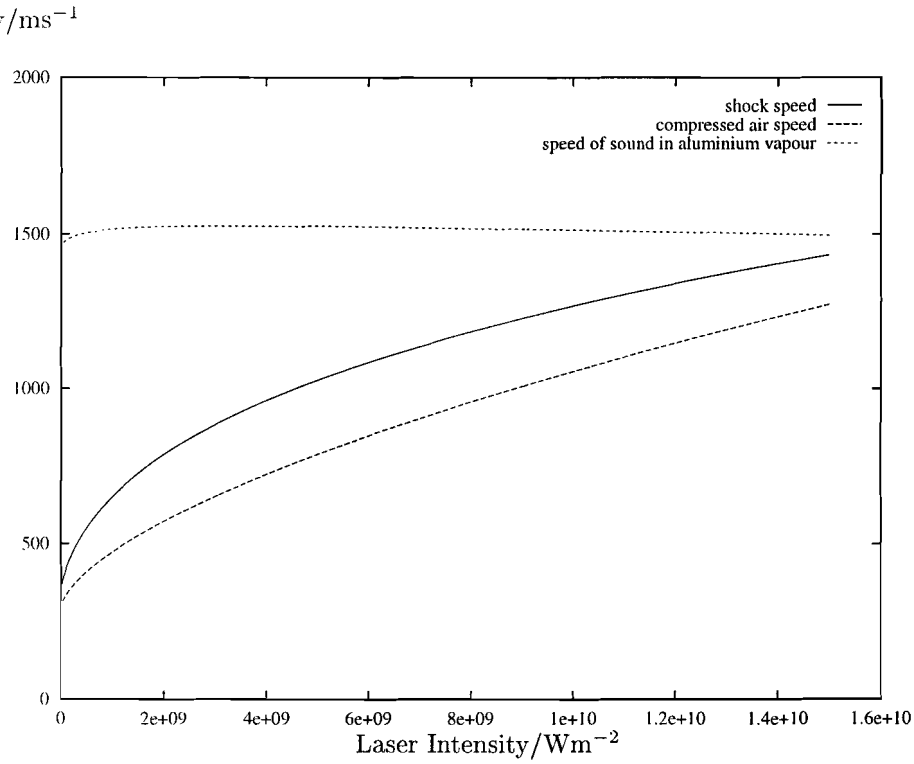

Figure 7: The shock speed, compressed air speed and speed of sound in the aluminium vapour as a function of laser intensity. The data is given in Table 3.

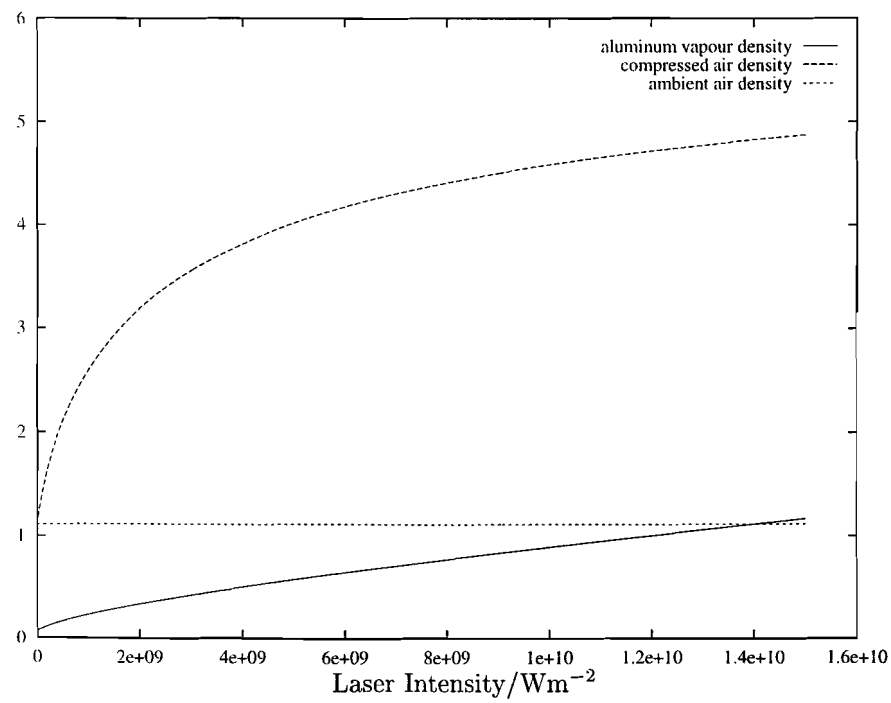

Figure 8: The aluminium vapour density, compressed air density and ambient air density as a function of laser intensity. The data is given in Table 3.